A CRACK-TRACKING TECHNIQUE FOR LOCALIZED DAMAGE IN QUASI-BRITTLE MATERIALS

Miguel Cervera [a] , Luca Pela' [b *] , Roberto Clemente [a] , Pere Roca [a]

[a] *International Center for Numerical Methods in Engineering (CIMNE), Technical University of Catalonia (UPC), Campus Norte, Jordi Girona 1-3, 08034 Barcelona, Spain.*

[b] *DISTART Department, University of Bologna, Viale Risorgimento 2, 40136 Bologna, Italy.*

Abstract - This work presents a procedure to simulate the growth and propagation of localized tensile cracks on quasi-brittle materials. The so-called smeared damage approach, which consists in standard finite elements and local nonlinear constitutive laws, is recovered and improved in order to represent crack localization and avoid spurious mesh-bias dependence in the discrete problem. This is achieved by means of the implementation of a local crack-tracking algorithm which can reproduce individual (discrete) cracks and ensure objectivity of the finite element problem solution. The performance of the localized damage model is stressed by means of the analyses of structural case-studies. Compared to the smeared crack approach in its original form, the presented procedure shows clearly a better capacity to predict realistic collapse mechanisms. The proposed tracking technique is relatively inexpensive.

Keywords: Continuum Damage Model, Strain Localization, Tensile Cracking, Crack-Tracking Technique, Quasi-Brittle Materials.

* Corresponding author.

E-mail addresses: miguel.cervera@upc.edu (Miguel Cervera), luca.pela@unibo.it (Luca Pela'), clemente@cimne.upc.edu (Roberto Clemente), pere.roca.fabregat@upc.edu (Pere Roca).

Nomenclature

A_e	Finite element area
$\mathbf{C}$	Isotropic linear-elastic constitutive tensor
d	Damage index
D	Specific dissipated energy
E	Young's modulus
f_0	Uniaxial tensile strength
G_f	Tensile fracture energy
h_e	Average element size
H_{dis}	Discrete softening parameter
H_{mat}	Material softening parameter
l_{dis}	Discrete crack characteristic width
l_e	Finite element size
l_{mat}	Material characteristic length
$\mathbf{p}_i$	Unit vector associated with *i*-th principal direction
r	Damage threshold internal variable
r_{excl}	Exclusion radius
r_{neigh}	Radius of the neighbourhood where V_c is computed
r_0	Initial value of the damage threshold internal variable
ν	Poisson's ratio
V_c	Crack average direction vector
$V_{c,\max}$	Vector which forms an angle $\alpha_{\max}$ with vector V_c
V_e	Crack direction vector for the current element
α	Angle between V_c and V_e
$\alpha_{\max}$	Maximum curvature angle
$\boldsymbol{\varepsilon}$	Strain tensor
Φ	Damage criterion
$\boldsymbol{\Lambda}$	Damage threshold surface shape tensor
$\boldsymbol{\sigma}$	Stress tensor
$\bar{\boldsymbol{\sigma}}$	Effective stress tensor

$\bar{\boldsymbol{\sigma}}^{+}$, $\bar{\boldsymbol{\sigma}}^{-}$	Tensile and compressive effective stress tensors
$\bar{\sigma}_i$	i-th principal effective stress
τ	Equivalent stress
:	Double contraction
$\langle . \rangle$	Macaulay brackets
Acronyms	
CMOD	Crack Mouth Opening Displacement
DCA	Discrete Crack Approach
E-FEM	Elemental enrichment Finite Element Method
FE	Finite Element
FEM	Finite Element Method
SCA	Smeared Crack Approach
X-FEM	eXtended Finite Element Method

1. Introduction

The numerical modelling of tensile cracking phenomena on quasi-brittle materials is one of the key topics in Computational Failure Mechanics. Two main difficulties have to be overcome in the discrete finite element (FE) problem: the representation of the opening crack, both in terms of displacement and/or strain fields, and the prediction of the direction for crack propagation.

With regard to the first issue, the most promising of the newly proposed methods are enhancements of the classical Discrete Crack Approach (DCA) and Smeared Crack Approach (SCA) [1].

In the Elemental enrichment Finite Element Method (E-FEM) [2-6] the displacement field at the crack is assumed to be discontinuous and the strain field is decomposed into a regular part, outside the crack, and a singular part at the crack. This, together with the explicit control on the energy dissipated in the formation of the crack, represents a link with the established tradition of Fracture Mechanics. Nevertheless, such approach does not really depart from the usual continuum framework.

The eXtended Finite Element Method (X-FEM) [7-10], when combined with level sets [11], is able to represent the discontinuity geometry, the displacement field across the crack and the developed singular field at the crack tip in terms of nodal values at the nodes of the mesh. The accuracy and the versatility of the approach are remarkable but a disadvantage lies in the special integration rules required inside the affected finite

elements to account for what happens at and outside the discontinuity. An exhaustive review about recent advances in X-FEM is reported in [12].

It has been observed in [13] that the computational cost in X-FEM is higher than in E-FEM and it increases even more in case of multiple cracks.

Integrated strategies with transition from Continuum Damage to macro-cracks simulated by means of X-FEM [14] or E-FEM [15] have been also proposed in order to correct initial mispredictions of the crack direction during its evolution.

Other options have been recently investigated. On one hand, in [16,17] the displacement discontinuity is replaced with a regularized approximation within the framework of the X-FEM. A meso-scale mesh-size independent "characteristic length" related to the process zone width is introduced. Therefore, the displacement and strain fields at the crack are continuous with continuous derivative, enabling one to adopt standard integration procedures instead of sub-elemental ones. On the other hand, in [18,19] a smeared-embedded continuum crack model is presented which incorporates the effect of the displacement jumps in the strain field of the elements, rather than the actual jumps themselves. Necessary corrections are introduced in the model to avoid mesh-size and mesh-bias dependency. The solution for the latter drawback is found in the form of a mesh corrected crack model, where the structure of the inelastic strain tensor is linked to the geometry of the cracked element. Such approach can be considered a particular case of the classical SCA, implemented at constitutive level.

Figures 1-2 sketch the comparison between the different approaches described, with relation to the crack modelling in the discrete FE model. The differences among them are subtle when referred to a 1D situation, but the different implications in 2D and 3D are significant, since it is necessary to establish the functional relationships between the fields of displacements (continuous and discontinuous) and strains (bounded and unbounded), and then with those of stresses. The displacement and strain fields at the crack represented by the strong discontinuity theories of E-FEM [2] and X-FEM [9] are depicted in Figure 1a, whereas their regularized versions are reported respectively in Figures 1b and 1c. Oliver *et al.* [4] use a "small" regularization length to obtain a bounded strain field at the discontinuity defined in terms of the displacement jump, measured as the difference of the displacement field at both sides of the band, see Figure 1b. This length may decrease during the deformation process according to an evolution law. Benvenuti [16] introduces a regularization length related to the width of the process zone that remains constant during the dissipative process and inside which

both the displacement and strain fields are continuous, see Figure 1c. Such regularized versions of E-FEM/X-FEM recall, in a certain sense, the classical SCA of Rashid [1], depicted in Figure 2a, even if in this case the characteristic length is equal to the relevant dimension of the finite element where the crack is to be represented. This similarity is exploited in the embedded SCA proposed by Cervera [18,19], see Figure 2b, where concepts developed for the E-FEM are incorporated in a SCA context.

With regard to the second issue mentioned at the beginning of this introduction, i.e. the prediction of the direction for crack propagation, it is deemed as the main difficulty to be overcome in the discrete FE problem.

In the classical SCA it has always been implicitly assumed that the criterion for the onset of cracking, which is established in terms of stresses/strains, also must automatically define the direction of propagation. This may be a natural assumption in the continuous problem, with proper evaluation of stress and strain values and directions. However, in the discrete problem the stress and strain fields evaluated in the vicinity of the crack tip differ greatly from being exact. Therefore, the computed damage distribution is incorrect, as it depends spuriously on the alignment of the finite element mesh. This error must be overcome if reasonable solutions are to be obtained with the SCA.

On the other hand, the application of E-FEM or X-FEM invariably needs the use of discontinuity tracking algorithms, in order to establish which elements lie in the crack path and need to be enriched [20-23]. Successful applications of such techniques point to the potential advantages of using a crack tracking algorithm in the discrete format of the crack propagation problem, also if continuous displacement fields are used in the interpolation basis.

The crack tracking technique marks the finite elements which can damage and prevents the others from failing. This essential feature

- minimizes the number of possible solutions, so it helps to identify the expected one;
- leads to a better representation of the expected solution for mixed-modes fracture problems, which are often characterized by curved cracks [24];
- avoids (or limits) the mechanical dissipation outside the crack track. A better description of the dissipative phenomenon is achieved by forcing the crack to develop along a single row of finite elements, since the elemental softening parameter is directly related to the fracture energy of the material.

The crack tracking algorithm to be used in crack propagation problems must be consistently linked to the cracking criterion, as this is the established cracking mechanism at continuum level. For a Rankine criterion based on the value of the maximum tensile principal stress, it is consistent to assume that the crack propagates in the plane orthogonal to the corresponding first stress eigenvector.

Non-local tracking strategies determine the crack path making reference not to local variables values but to their non-local counterparts, accounting for the influence of the neighbourhood on a certain material point [25,26]. Non-local averaging techniques are rather cumbersome since the modular element-wise nature of finite element analyses is spoiled. As a consequence, the complexity of implementation is relatively high.

A global crack tracking technique has been proposed by Oliver and co-workers [5,6] within the framework of E-FEM and combined with the SCA by Cervera & Chiumenti [24,27] afterwards. Such a methodology considers the evaluation of the propagation direction as a separate problem, independent from the local values of the discrete stress/strain fields. The direction of propagation is evaluated by solving a conduction-like problem which, by definition, is sufficiently well-behaved and does not present any singular point in the vicinity of the advancing crack. However, the solution of such additional problem for each mechanical loading step involves some programming complexity and additional computational cost. As a remedy for these drawbacks, a partial domain crack tracking algorithm has been employed [15,28] in which the scalar field with isolines is constructed only for the domain which actually is or potentially will be affected by the discontinuity. A practical comparison between different crack path tracking techniques is reported in [29].

This work deals with an enhanced local crack-tracking algorithm, in which the propagation direction is evaluated locally and corrected opportunely depending on potentially damaging and already damaged elements on the crack [30]. Such innovative tool, combined with a continuum damage constitutive law with strain-softening, provides a numerical model for the solution of problems involving tensile cracking in quasi-brittle materials, such as concrete and masonry [31]. Unlike with the use of the standard SCA, the resulting damage in the ultimate conditions appears localized in individual cracks, represented via continuous paths. Moreover, the results do not suffer from spurious mesh-size or mesh-bias dependence. The proposed model is much less computationally intensive than the similar one used in [24,27], which is based on a global crack-tracking technique.

The paper is organized as follows: first, a brief review of the local continuum damage model is reported; then, the proposed local crack-tracking technique is discussed in detail. Finally, the numerical tool is validated via the FE analyses of relevant structural examples.

2. Local Continuum Damage Model

In this work a constitutive model based on the Continuum Damage Mechanics theory is considered. Since the adopted formulation is mostly identical to the one described in [27], it will be briefly summarized hereinafter, referring the reader to the cited paper for any further detail.

2.1 Constitutive Model

The constitutive equation for the damage model is defined as

$$\boldsymbol{\sigma} = (1-d)\,\bar{\boldsymbol{\sigma}} = (1-d)\,\mathbf{C} : \boldsymbol{\varepsilon} \tag{1}$$

where the effective stress $\bar{\boldsymbol{\sigma}}$ [32] can be computed in terms of the total strain tensor $\boldsymbol{\varepsilon}$, $\mathbf{C}$ is the usual (fourth order) isotropic linear-elastic constitutive tensor and d is the damage index, i.e. an internal-like scalar variable equal to zero when the material is undamaged and equal to one when it is completely damaged.

As our aim is to use a scalar damage model sensitive only to tensile stresses contributions, a split of the effective stress tensor into tensile and compressive components is carried out according to [33]:

$$\bar{\boldsymbol{\sigma}}^{+} = \sum_{i=1}^{3} \langle \bar{\sigma}_i \rangle \, \mathbf{p}_i \otimes \mathbf{p}_i \quad \text{and} \quad \bar{\boldsymbol{\sigma}}^{-} = \bar{\boldsymbol{\sigma}} - \bar{\boldsymbol{\sigma}}^{+} \tag{2}$$

where $\bar{\sigma}_i$ denotes the i-th principal stress value from tensor $\bar{\boldsymbol{\sigma}}$, $\mathbf{p}_i$ represents the unit vector associated with its respective principal direction and the symbols $\langle . \rangle$ are the Macaulay brackets $\left(\langle x \rangle = x, \, if \; x \geq 0, \langle x \rangle = 0, \, if \; x < 0\right)$.

The scalar positive quantity, termed as equivalent stress τ, is defined in order to identify “loading”, “unloading” or “reloading” situations for a general 3D stress state, according to:

$$\tau = \left[\bar{\boldsymbol{\sigma}}^{+} : \boldsymbol{\Lambda} : \bar{\boldsymbol{\sigma}}^{+} \right]^{1/2} \tag{3}$$

The shape of the damage threshold surface in the effective stress space is defined by the non-dimensional fourth order tensor $\mathbf{\Lambda}$, which is assumed in this work equal to

$$\mathbf{\Lambda} = \mathbf{p}_1 \otimes \mathbf{p}_1 \otimes \mathbf{p}_1 \otimes \mathbf{p}_1 \tag{4}$$

leading to the well-known Rankine criterion in tension.

If one designates by *r* the greatest values (here termed as threshold) ever reached until an instant *t* by the equivalent stress τ, increments of the damage variable *d* during time interval $[t,\ t+\Delta t]$ are assumed to occur only when $\tau_{t+\Delta t} > r_t$ (see [34] for details). Accordingly, the following damage criterion is introduced:

$$\Phi(\tau, r) = \tau - r \leq 0 \tag{5}$$

Based on Equations (3) and (5), the initial elastic domain is defined by the condition $\tau = r_0$, where $r_0 = f_0$, being f_0 the stress that defines the onset of nonlinearity on 1D tension.

2.2 Strain softening and discrete crack width regularization

The damage index $d = d(r)$ is explicitly defined in terms of the corresponding current value of the damage threshold *r*, so that it is a monotonically increasing function such that $0 \leq d \leq 1$. In this work, the softening law takes the following exponential form [35]

$$d(r) = 1 - \frac{r_0}{r} \exp\left\{ 2\, H_{dis} \left(\frac{r_0 - r}{r_0} \right) \right\} \tag{6}$$

where constant $H_{dis} \geq 0$ is the discrete softening parameter.

Since Bazant and Oh [36] it was recognized that the use of constitutive laws with softening in the SCA leads to solutions strongly dependent on the mesh refinement. In order to ensure mesh-size objective results, the discrete softening law has to be modified in such a way that the energy dissipated over a completely degraded finite element is equal to a given value, which depends on the material fracture energy and on the element size. Accordingly, the specific dissipated energy *D* is adjusted for each FE in the crack band, so that the equation

$$D \cdot l_{dis} = G_f \tag{7}$$

applies, where G_f is the material tensile fracture energy and l_{dis} is the discrete crack characteristic width, i.e. the computational width of the fracture zone. This can be derived according to the consistent methodology suggested by Oliver [37].

For the damage model with the exponential softening it can be proved that the specific dissipated energy is

$$D = \left(1 + \frac{1}{H_{dis}}\right)\frac{\left(f_0\right)^2}{2E} \tag{8}$$

and, therefore, using (7) and (8) the discrete softening parameter is defined as

$$H_{dis} = \frac{l_{dis}}{l_{mat} - l_{dis}} \tag{9}$$

where the material characteristic length is $l_{mat} = 1/H_{mat}$, with $H_{mat} = \left(f_0\right)^2 / \left(2E G_f\right)$ depending only on the material properties.

It has to be remarked that this regularization procedure does not apply to the continuum format of the cracking problem. If discontinuous displacements are considered in the continuous problem, the nonlinear constitutive behaviour can be established in terms of a traction-versus-jump law. If the discrete problem reproduces the displacement jumps, as it happens in the E-FEM/X-FEM, then no regularization procedure is necessary (Figure 1a), although it is also used in the regularized versions of these formulations (Figures 1b and 1c). Contrariwise, in the SCA, mesh-size regularization is necessary because of the smearing of the displacement jump over the resolution length which the FE mesh is able to achieve (Figure 2). Obviously, this only refers to the discrete problem, and it depends on the element size. It is important to note that when the mesh is refined the continuous constitutive model is recovered as a limit case.

In the framework of local models and FE analysis, the state variables are computed at the integration points in terms of the local strain (and/or stress) history. Therefore, the discrete crack characteristic width is related to the volume (or area) of each finite element [38]. For linear simplex elements, the discrete crack characteristic width can be taken as the representative size of the element, $l_{dis} = l_e$. In this work, and assuming that the elements are equilateral, the size of the element will be computed as $l_e^2 = \left(4/\sqrt{3}\right) A_e$ for triangular elements.

3. Local Crack-Tracking Technique

Although the problem of mesh-size dependence in SCA has been satisfactorily overcome, as mentioned in Section 2.2, the issue concerning the mesh-bias dependence of the FE solution still remains unsolved. It is well-known that only if the spatial discretization is designed in such way that an "appropriate" path for the advancing crack is available, the SCA solution results satisfactory. In this work, a solution to the problem is found by making use of a crack-tracking technique.

The local crack-tracking algorithm detects the point where a crack is originated and then it lets the crack propagate perpendicularly to the trajectory of the first principal tensile stress. The algorithm marks the finite elements pertaining to the crack path which can experience potential damage. The crack is forced to develop along a single row of finite elements. The regularization procedure using the material properties and the element characteristic length ensures that dissipation will be element-size independent, see Equation (7).

The proposed method is applied at every time step during the analysis, just before the stress evaluation. The method works with a flags system, where finite elements are labelled to delimit the zones where cracks will appear or develop. The criteria used to define these zones depend on the magnitude and direction of the principal stresses at each element. The algorithm has been implemented for 2D problems using three-noded standard elements with continuous displacement field. Despite their well-known approximability limitations, constant strain-triangles ensure an efficient implementation. The procedure is divided into two steps. First, new cracks are detected by checking the stress values at every finite element located on the boundary of the structure. Then, the track of finite elements pertaining to the crack path is marked by the algorithm, in order to compute the crack propagation direction.

3.1 New Crack Detection

The input data of this first stage of the procedure are (i) the principal tensile stress values of the elements located on the boundary of the mesh and (ii) the list of the elements labelled as "crack root", all referred to the previous time step.

Then, the following operations are carried out:

1. New elements are labelled as potential crack roots. For this aim, we consider some criteria:

- The crack starts once the principal tensile stress value reaches the material strength, according to the Rankine tensile criterion. This check is performed only on finite elements located on the boundary of the mesh. Therefore, cracks are assumed to start only from the border of the structure.
- When several neighbour elements reach the tensile strength at the same time step, the exclusion radius criterion is applied. This radius r_{excl} (defined by the user) is the minimum distance imposed between two crack root elements, and it is used to guarantee the creation of separated discrete cracks. Among all the elements which have reached the tensile strength at the same time step, and which are contained into the exclusion radius, the one with the greatest principal tensile stress is labelled as crack root.

2. The spatial coordinates of the crack origin are computed. The midpoint of the element side located at the mesh boundary is considered. In case of corner elements, the centroid is assumed, see Figure 3.

The output data of the new cracks detection procedure is the list of the potential crack root elements, together with their spatial coordinates.

3.2 Crack Propagation

The input data of this second stage of the procedure are (i) the list of the potential crack root elements, together with their spatial coordinates, (ii) the principal tensile stress values and directions of all the mesh elements and (iii) the list of the elements belonging to consolidated cracks referred to the previous time step.

Then, the following operations are carried out:

1. Determine the “tip of the crack element” for each existing consolidated crack. This is defined as the damaged element with only one neighbour damaged element.
2. For each tip of the crack element, as well as for the new crack root elements, the following processes are executed:
   - Determine the exit point coordinates. A vector is drawn from the entry point coordinates (defined below), using the direction perpendicular to the principal tensile direction of the element. The exit point is defined as the intersection of that vector with the corresponding face of the element, see Figure 4a.

- Determine the next potential element on the crack for the current time step. This is the neighbouring element whose face in common with the current element corresponds with the face where its exit point is located. The element is marked as a potential element belonging to this crack.
- Determine the entry point coordinates. The entry point of the new element on the crack is located at the same coordinates of the exit point of the previous element, see Figure 4b.
- Repeat the three previous steps, taking the new potential element as the crack tip element.

For each crack, the previous procedure is repeated until one of the following criteria is satisfied:

- *Stress threshold criterion*. Element tracking and labelling is stopped when the principal tensile stress is lower than a threshold defined by the user. The experience has demonstrated that 75% of tensile strength usually works well.
- *Crack meeting criterion*. The procedure stops when a previously damaged element, or an element marked as a potentially cracking one, is found along the current crack. This means that two cracks have met, and from then on they will be considered as a single one.
- *Boundary criterion*. When the exit point of an element is on the boundary of the structure, the cracking process finishes.

3. Once any of the previous criteria is reached, the current crack is considered totally developed and the next one is studied, by restarting the cycle. Finally, after applying this procedure to all the cracks, each element will have one of the three following labels:
    - Intact element, not able to damage (out of potential crack track; it will keep elastic behaviour during the current time step)
    - Intact element, able to damage (in a potential crack track; it will initiate inelastic behaviour if the material strength is reached)
    - Damaged element (belonging to a crack consolidated in previous time steps; it will develop inelastic behaviour during the rest of the calculations)

The analysis procedure recognizes these labels and activates the corresponding constitutive law (elastic or damage) in each element for the current time step. Also, once the stresses have been updated and the damaged indexes are known, the elements with potential cracking that really suffer damage are relabelled as included in a consolidated

crack for the rest of calculations. Finally, elements potentially cracking that do not suffer damage are restored to their original status, i.e. unlabelled.

The proposed algorithm, based on the directions of the stresses in the previous time step, is of first order accuracy (the error is proportional to the size of the time step). More accurate algorithms can be formulated. For instance, a second order prediction on the stresses at the current time step can be done in terms of the stresses at the two previous time steps. Such procedure would reduce the dependence of the computed crack track on the size of the time step significantly, particularly in the case of curve crack trajectories.

3.3 Maximum Curvature Criterion

The implementation of the crack tracking algorithm in the form described just in Sections 3.1.1 and 3.1.2 leads to some problems in case of bending stress states. Figure 5 shows the FE simulation of an advancing flexural crack in the middle of a 3-point loaded concrete beam. The contour of tensile damage is zoomed in the proximity of the neutral axes, as well as the tensile principal directions (red arrows). As can be seen, since the algorithm assumes the direction of the crack to be perpendicular to the principal tensile stress, the track should propagate from the crack tip (element A) to element B and then to element C. This is obviously erroneous, because the vertical crack should go up to the element D. Therefore, the local crack tracking technique needs a specific device to overcome such a drawback.

In this paper, the maximum curvature criterion is introduced in order to correct spurious changes of propagation direction. The procedure consists in identifying and correcting the sudden change of curvature in the crack track, before marking each potential element. Making reference to Figure 6a, the following parameters are considered:

- Crack direction vector for the current element V_e.
- Crack average direction vector V_c. It is equal to the vectorial sum of the elemental cracking vectors. The elements considered in the calculations are those potential at the current time step and those consolidated at the previous time steps whose centroids lie inside a neighbourhood of radius r_{neigh}. Such length is defined by the user and it is measured from the centroid of the current tip element (see Figure 6b).
- Angle α between V_c and V_e.

- Maximum curvature angle $\alpha_{\max}$, defined by the user at the beginning of the calculations.
- Vector $V_{c,\max}$ which forms an angle $\alpha_{\max}$ with vector V_c.

If it results that $\alpha \le \alpha_{\max}$, the considered element is marked as potential for the current time step with a corresponding direction V_e. Then, the following element of the crack is considered.

If it results that $\alpha > \alpha_{\max}$, the crack direction is deflecting sharply (see Figure 6a) and a correction is carried out, using V_c instead of V_e. This means to impose the crack the average direction exhibited until the step considered with respect to a specified neighbourhood of radius r_{neigh} (see Figure 6b). In the case of problems involving straight or small curvature cracks, the choice of r_{neigh} obviously does not affect particularly the crack direction prediction. In the case of problems with curved cracks, on the other hand, vector V_c has to be computed making reference to a limited number of FEs in order to simulate correctly the curvature of the propagating crack. Therefore, the choice of r_{neigh} may influence the results accuracy, as it will be shown in Section 4.3.

Once the crack direction correction is carried out, the standard procedure is followed, i.e. the element is marked as potential and the new one is considered.

It is worth mentioning that crack tracking algoritms are sensitive to the precision achieved in the computed values of the stresses (or strains) at the root of the crack. Point-wise convergence on the stress (or strain) values for a given FE formulation is a research topic which deserves in-depth investigation.

4. Validation Examples

In this Section, the proposed localized damage model based on a crack-tracking technique is validated by means of numerical structural examples. First, a simple benchmark example consisting in a holed strip subjected to uniaxial tension is analyzed. The second validation example is a three point bending test on a concrete beam. Then, a more complicated case study is considered, that is the simulation of a mixed-mode bending test on a concrete beam. Finally, the analysis of a masonry semicircular arch is presented, for the particular case of asymmetrical vertical load.

Calculations are performed with an enhanced version of the finite element program COMET [39], developed at the International Centre for Numerical Methods in Engineering (CIMNE, Barcelona). The problem is solved incrementally in a (pseudo) time step-by-step manner. Within each step, a modified Newton–Raphson method (using the secant stiffness matrix), together with a line-search procedure, is used to solve the corresponding non-linear system of equations. Convergence of a time step is attained when the ratio between the norm of the iterative residual forces and the norm of the total external forces is lower than 1%. Pre- and post-processing are done with GiD [40], also developed at CIMNE.

4.1 Holed Strip under Uniaxial Traction

The numerical analysis of a holed strip subjected to uniaxial stretching is considered, in order to point out the difference between a traditional smeared damage model and its enhanced version improved by a crack tracking algorithm.

This example has been already solved in [27] making use of a global crack-tracking technique. The same material data are considered: Young's modulus $E = 30\,\text{GPa}$, Poisson's ratio $v = 0.2$, tensile strength $f_0 = 2\,\text{MPa}$ and mode I fracture energy $G_f = 100\,\text{J}/\text{m}^2$. The specimen size is 200 x 400 mm^2 and the radius of the perforation is equal to 10 mm. Axial vertical displacements are applied to both the strip ends. Since the problem is symmetrical, only the right half of the computational domain is considered and discretized in two different unstructured meshes with average mesh sizes of $h_e = 5\,\text{mm}$ (2023 nodes) and $h_e = 2.5\,\text{mm}$ (7648 nodes). The problem is analyzed assuming two-dimensional plane strain conditions.

First, the traditional smeared damage model is considered in calculations. Figure 7 shows the computed deformed shapes and tensile damage contours in the two different meshes for a (half)-imposed vertical displacement of 0.1 mm. As shown, the crack grows from the perforation, then it propagates horizontally and it suddenly deviates from the expected correct path, following a line of FEs inclined of about 30°. This result is definitely spurious and strongly dependent on the considered spatial discretizations.

Then, the damage model based on a local crack-tracking technique is adopted in the analyses. The choice of the tracking parameters is irrelevant in this example. In fact, r_{excl} definition is not necessary since a unique crack is expected. No correction of the

crack direction is required because the stress field is uniformly uniaxial, so $\alpha_{\max}$ and r_{neigh} are irrelevant.

Figure 8 shows how the crack propagates correctly along the horizontal axis of symmetry, without following any "favourable" path given by the considered meshes. Figure 9 shows the (half)-load vs. (half)-imposed vertical displacement curves obtained in the two analyses with local crack-tracking technique. As shown, the results are remarkably mesh-size independent.

It is worth noticing that the results presented in Figures 8-9 are identical to the ones obtained in [27] by a global crack-tracking technique because the meshes used are the same and both the algorithms predict exactly a horizontal crack. Nevertheless, the global tracking approach is more computationally expensive than the local one, since it is necessary to solve a conduction-like problem at each step of the analysis. The local crack-tracking algorithm, on the other hand, stands out because of its efficiency and lower computing time. In fact, if the analysis with $h_e = 2.5\,\text{mm}$ is run in a standard PC equipped with a single Pentium 4 – 3.2 GHz, 2 GB Ram – processor, the absolute CPU time results equal to 194.97 seconds using the global tracking and equal to 148.19 seconds using the local tracking. Since the computing time for the classical SCA is equal to 132.98 seconds, the additional calculation effort for the local crack-tracking is only 24.5 % of that required for the global one.

4.2 3-point Bending Beam

The second example is a three point bending test on a notched concrete beam [41] whose dimensions and boundary conditions are given in Figure 10. The behaviour of the proposed local crack-tracking algorithm in bending problems is investigated, as well as the influence of the load step size.

The mesh is constituted by 2380 elements and 1248 nodes. The FEs average size is $h_e = 2\,\text{mm}$ in the proximity of the cracking zone. The two adopted load incrementation strategies consist of 100 and 1000 load steps; accordingly, the vertical displacement $\delta = 1\,\text{mm}$ is applied in the midpoint through steps of magnitude $1\times10^{-2}\,\text{mm}$ and $1\times10^{-3}\,\text{mm}$. The material data are: Young's modulus $E = 20\,\text{GPa}$, Poisson's ratio $v = 0.2$, tensile strength $f_0 = 2.4\,\text{MPa}$ and mode I fracture energy $G_f = 113\,\text{J}/\text{m}^2$. The beam has thickness equal to 100 mm and it is analyzed under two-dimensional plane strain assumptions.

As explained in Section 3.3, the maximum curvature criterion is necessary in the case of flexure problems to avoid the crack "about-turn" phenomenon (Figure 5). Accordingly, several FE analyses have been executed in order to assess the influence of $\alpha_{\max}$ on the results. With a step magnitude of $1\times10^{-2}\,\text{mm}$, values $\alpha_{\max}\le 50°$ predict the correct crack direction, see Figure 11. For greater values of $\alpha_{\max}$, the predicted crack suffers from sharp changes of direction during its propagation, leading to incorrect results. For a smaller step magnitude of $1\times10^{-3}\,\text{mm}$, the aforementioned upper limit increases to $\alpha_{\max}\le 60°$.

Figure 12 shows the comparison between the experimental [41] and the numerical load-displacement curves. Note that the curves obtained with the two different load step sizes tally very closely. Good agreement is achieved, both in terms of load peak value and energy dissipation in the nonlinear range.

Definition of r_{excl} is not necessary in this example since it presents a unique crack. Also, an adequate number of neighbour elements is selected with $r_{neigh}\ge 10\,\text{mm}$ in order to reproduce the correct straight direction of the crack.

4.3 Mixed-Mode Bending Beam

The third example is a plane-strain notched beam subjected to mixed-mode bending test. The experimental evidence reported in [42] is simulated by means of the proposed model. Figure 13 depicts the geometry of the problem and the boundary conditions applied to the concrete beam. In a first case the stiffness at the upper left support is assumed equal to zero ($K=0$, i.e. a three point bending beam), while in a second case is infinite ($K=\infty$, i.e. a four point bending beam). The load *P* is applied by imposing vertical displacements. The following material properties are assumed for concrete: Young's modulus $E=38\,\text{GPa}$, Poisson's ratio $\nu=0.2$, tensile strength $f_0=3\,\text{MPa}$ and mode I fracture energy $G_f=69\,\text{J/m}^2$. The computational domain is discretized in 13443 triangular elements, with a total number of 7028 nodes. The average mesh size in the zone interested by the tensile fracture is $h_e=2.5\,\text{mm}$.

Figure 14 shows the computed deformed shapes at collapse obtained assuming $\alpha_{\max}=20°$ for the specimen 1 (three point test) and $\alpha_{\max}=32°$ for the specimen 2 (four point test). In the former analysis it is assumed $r_{neigh}=5\,\text{mm}$ while in the latter $r_{neigh}=10\,\text{mm}$. The definition of r_{excl} is not necessary in these examples since they

present a unique crack. Figure 15 shows the comparisons between the experimental and the numerical crack tracks, in which it is possible to appreciate a remarkable agreement. Figure 16 presents the Load vs. CMOD curves for specimens 1 and 2. In the first case (Figure 16a), the numerical curve is quite similar to the experimental ones, even if the numerical model slightly underestimates the strength in the last part of the calculus. In the second test (Figure 16b), the concordance of numerical result with the experimental evidence is clear, until a sudden collapse occurs for $\mathrm{CMOD} = 0.11\,\mathrm{mm}$.

For specimen 2, a maximum curvature angle $\alpha_{\max} = 32°$ has been chosen in order to avoid sharp changes of the crack direction. Since the crack is straight, the assumed value $r_{neigh} = 10\,\mathrm{mm}$ is irrelevant for the result shown in Figure 14b.

A sensitivity analysis regarding the parameters used for the tracking algorithm has been carried out for specimen 1, because it presents an interesting case of a crack with a certain curvature. The first parameter which has been investigated is $\alpha_{\max}$ because it plays a key role in the crack direction correction through the maximum curvature criterion, as shown in Section 4.2. Values of $\alpha_{\max} \leq 55°$ are necessary to avoid sharp changes of the crack direction. Below this upper-bound value, some variations in the numerical crack track can be appreciated for $\alpha_{\max} = 40°$ and then for $\alpha_{\max} = 20°$. It is noticed that there is an initial length of the crack of about 40 mm which is insensitive to the variation of the tracking parameters. It is at this distance from the notch where the algorithm comes into play. This is evident in Figure 17, where the computed crack tracks (depicted by the damaged elements) can be compared to the experimental envelope. Once the crack "about-turn" phenomenon is avoided, thanks to the restriction imposed by $\alpha_{\max}$, the effect of the choice of r_{neigh} is investigated. Results corresponding to values of r_{neigh} = 20, 10 and 5 mm are shown. Values of $r_{neigh} > 20\,\mathrm{mm}$ yield the same results as with $r_{neigh} = 20\,\mathrm{mm}$. On one hand, Figure 17 shows that for $r_{neigh} = 20\,\mathrm{mm}$ the resulting crack track is almost straight. Values of $r_{neigh} = 10\,\mathrm{mm}$ or $r_{neigh} = 5\,\mathrm{mm}$, on the other hand, allow the crack to change direction during propagation. For $\alpha_{\max} = 20°$ and $r_{neigh} = 5\,\mathrm{mm}$ the numerical crack track lies entirely inside the experimental envelope.

4.4 Asymmetrically Loaded Semicircular Arch

The fourth example consists in a semicircular arch with thickness and width equal to 1 m and a radius of 5 m. Both the supports are fixed and a vertical load is applied

according to the scheme reported in Figure 18a. The following material properties are considered for masonry: Young's modulus $E = 5\,\text{GPa}$, Poisson's ratio $v = 0.2$, tensile strength $f = 0.2\,\text{MPa}$ and mode I fracture energy $G_f = 10\,\text{J}/\text{m}^2$. All the numerical analyses are carried out under the hypothesis of plane strain, with unitary thickness assumed. Gravitational loads are applied to the arch, before a vertical load is monotonically increased by considering load steps of 3 kN in the case of force control or increments of 0.05 mm under displacement control. The computational domain is discretized in 11324 triangular elements, with a total number of 5989 nodes and a average mesh size $h_e = 50\,\text{mm}$.

Before the numerical analyses, a static limit analysis has been carried out in order to assess the ultimate load value (about 150 kN) and the position of the plastic hinges, defined by letters A-D in Figure 18b. Such results have been also validated through the RING software [43].

Then, the masonry arch behaviour is studied by means of the traditional smeared damage approach, considering both the load and the displacement control analyses. Figure 19 shows the curve of load vs. vertical displacement in the application point of force *P*. As can be seen, the ultimate load calculated value is quite similar to the one derived by the limit analysis.

Figure 20 presents the damage distribution at stages 1-5 (refer to Figure 19) of the calculus carried out under force control. The attention is focused on the locations where a hinge development is expected, i.e. the points A-D of Figure 18b. The structural behaviour remains linear until $P = 110\,\text{kN}$, which corresponds to stage 1. Damage occurs first at points B and D, which are subjected to the highest values of tensile stress. Then, a sudden extension of the damaged zone arises in such points, as shown at stage 3. At stage 4, cracks B and D still remains radially oriented, while at points A and C a quite distributed damage occurs at the extrados. At stage 5, crack C progresses downwards and spreads over a quite extended region, similar to a bulb. After stage 5, as soon as crack A occurs, sections B, C and D damage completely and the arch collapse mechanism is activated. No more equilibrium points are found under load control.

Figure 21 presents the results of the analysis under displacement control. Compared to the previous analysis, it is possible to detect the unloading occurring after the formation of cracks B and D (branch 1-2 of Figure 19). At stage 2, crack B is not as spread as the equivalent one obtained under load control. Therefore, it is possible to conclude that in the smeared damage approach the solution depends on the particular loading path

followed. Another unloading occurs after the formation of cracks A and C (branch 4-6 of Figure 19). As shown in Figure 21, both the cracks follow a path given by the spatial discretization adopted. Therefore, it is evident the spurious mesh-bias dependence of the solution. After stage 6, the structure still presents a low stiffness, until another unloading is discovered (point 7 of Figure 19), which corresponds to the formation of a hinge in B (see Figure 21, in which crack B is shown before and after the jump).

Finally, the arch is analyzed by considering the localized damage model with crack-tracking technique. The following correction parameters are assumed for the maximum curvature criterion: $\alpha_{\max} = 30°$ and $r_{neigh} = 300\,\text{mm}$. The former has been chosen in order to avoid spurious changes of cracks direction, whereas the latter is the minimum value necessary to reproduce correctly the radial direction of cracks. The exclusion radius r_{excl} has been assumed equal to 3000 mm, making reference to the positions of the plastic hinges derived from the previous limit analysis. However, values within the wide range $1500\,\text{mm} \le r_{excl} \le 3200\,\text{mm}$ lead to a correct prediction of the hinges positions.

Figure 22 shows the curve of load vs. vertical displacement in the application point of force *P*. In the case of displacement control, the model is able to capture the unloading occurring after the formation of the first crack, denoted by branch 2-3. It is worth noticing that from point 4 the response of the analyses under force or displacement control are almost the same, as well as the cracks growth (Figure 23a) and the collapse mechanism (Figure 23b). Moreover, the damage distribution computed thanks to the tracking technique does not follow the mesh-bias, ensuring the correct expected solution of radial cracks.

5. Conclusions

This paper presents a local crack-tracking technique for the numerical modelling of tensile cracks in quasi-brittle materials. The classical smeared crack approach is improved by forcing the crack to develop along a single row of finite elements, as a function of the direction of the principal tensile stress. The algorithm works with a flag system where the finite elements which are allowed to damage during the current time step are appropriately labelled.

The proposed model has shown the following remarkable features:

- The simulation of the damage distribution in ultimate conditions is more realistic than in the classical SCA. The localized cracks predicted by the tracking model

reproduce consistently the ones usually experienced by concrete or masonry structures, which develop gradually and lead to the full collapse mechanism.

- Compared to the classical SCA, it does not require a significant additional computation cost. Compared to the global crack-tracking techniques, the proposed algorithm requires a less intensive computational effort.
- The dissipation is element-size independent due to the regularization procedure dependent on the material properties and the characteristic length.
- The analysis results are mesh-bias independent, ensuring the solution objectivity when different orientations of the mesh are considered in the discrete problem.
- The crack track correction, performed according to a maximum curvature criterion, avoids the spurious changes of propagation direction which are usual in bending dominated problems.
- The validation examples have shown the efficiency and the robustness of the local crack-tracking technique, which turns out to be suitable for tension and mixed-mode cracking problems.

The sensitivity analyses with respect to the tracking parameters $\alpha_{\max}$, r_{neigh} and r_{excl} have assessed their influence on numerical solutions:

- The maximum curvature angle $\alpha_{\max}$ is the most influential parameter, since it prevents the crack from turning back in bending problems. The relative independence of the results with respect to the chosen value for $\alpha_{\max}$ has been demonstrated, even for different load steps.
- The definition of r_{neigh} is useful to reproduce the correct track of curved cracks. It can be interpreted as a refinement parameter for crack track correction.
- The exclusion radius r_{excl} is necessary in multi-crack problems in order to represent the correct failure mechanism.

Given the sensitivity of the obtained crack paths on the selected parameters ($\alpha_{\max}$ in particular), sensitivity analyses similar to the ones conducted in the paper are advisable when the proposed tracking algorithm is used to predict crack tracks without the help of known experimental results. This remark is of course applicable to any of the existing crack tracking algoritms. Sensitivity analyses are almost mandatory in nonlinear computations in order to assess the reliability of the results obtained.

6. Acknowledgments

The studies presented here have been developed within the research projects BIA2006-04127 and SEDUREC (CSD2006-00060), funded by DGE of the Spanish Ministry of Science and Technology, whose assistance is gratefully acknowledged.

7. References

[1] Rashid Y. Analysis of prestressed concrete pressure vessels. Nucl Engrg Des 1968; 7:334-344.

[2] Simó J.C., Oliver J., Armero F. An analysis of strong discontinuities induced by strain-softening in rate-independent inelastic solids. Comput Mech 1993; 12:49–61.

[3] Oliver J. Continuum modeling of strong discontinuities in solid mechanics using damage models. Comput Mech 1995; 17:277–296.

[4] Oliver J., Cervera M., Manzoli O. Strong discontinuities and continuum plasticity models: the strong discontinuity approach. Int J Plast 1999; 15:319–351.

[5] Oliver J., Huespe A.E., Samaniego E., Chaves W.V. Continuum approach to the numerical simulation of material failure in concrete. Int J Numer Anal Methods Geomech 2004; 28:609–632.

[6] Oliver J., Huespe A.E. Continuum approach to material failure in strong discontinuity settings. Comput Methods Appl Mech Engrg 2004; 193:3195–3220.

[7] Belytschko T., Black T. Elastic crack growth in finite elements with minimal remeshing. Comput Methods Appl Mech Engrg 1999; 45(5):601–620.

[8] Möes N., Dolbow J., Belytschko T. A finite element method for crack growth without remeshing. Int J Numer Methods Engng 1999; 46:131–150.

[9] Möes N., Belytschko T. Extended finite element method for cohesive crack growth. Engng Fract Mech 2002; 69:813–833.

[10] Sukumar N., Möes N., Moran B., Belytschko T. Extended finite element method for three-dimensional crack modelling. Int J Numer Methods Engng 2000; 48:1549–1570.

[11] Sethian J.A. Level Set Methods and Fast Marching Methods. Cambridge University Press, Cambridge, 1999.

[12] Belytschko T., Gracie R., Ventura G. A Review of Extended/Generalized Finite Element Methods for Material Modelling. Modell Simul Mater Sci Eng 2009; 17(4):1-31.

[13] Oliver J., Huespe A.E., Sánchez P.J. A comparative study on finite elements for capturing strong discontinuities: E-FEM vs X-FEM. Comput Methods Appl Mech Engrg 2006; 195:4732–4752.

[14] Comi C., Mariani S. and Perego U. An extended FE strategy for transition from continuum damage to mode I cohesive crack propagation. Int J Numer Anal Methods Geomech 2007; 31:213–238.

[15] Theiner Y, Hofstetter G. Numerical prediction of crack propagation and crack widths in concrete structures. Eng Struct 2009; 31:1832-1840.

[16] Benvenuti E. A regularized XFEM framework for embedded cohesive interfaces. Comput Methods Appl Mech Engrg 2008; 197:4367–4378.

[17] Benvenuti E., Tralli A., Ventura G. A regularized XFEM model for the transition from continuous to discontinuous displacements. Int J Numer Methods Engng 2008; 74:911–944.

[18] Cervera M. A smeared-embedded mesh-corrected damage model for tensile cracking. Int J Numer Methods Engng 2008; 76:1930–1954.

[19] Cervera M. An orthotropic mesh corrected crack model. Comput Methods Appl Mech Engrg 2008; 197:1603–1619.

[20] Oliver J., Huespe A.E., Samaniego E., Chaves E.W.V. On strategies for tracking strong discontinuities in computational failure mechanics. In: Proceedings of the Fifth World Congress on Computational Mechanics, 2002.

[21] Mosler J., Meschke G. Embedded crack vs. smeared crack models: a comparison of elementwise discontinuous crack path approaches with emphasis on mesh bias. Comput Methods Appl Mech Engrg 2004; 193:3351–3375.

[22] Meschke G., Dumstorff P. Energy-based modeling of cohesive and cohesionless cracks via X-FEM. Comput Methods Appl Mech Engrg 2007; 196:2338–2357.

[23] Ventura G., Budyn E., Belytschko T. Vector level sets for description of propagating cracks in finite elements. Int J Numer Methods Engng 2003; 58:1571–1592.

[24] Cervera M., Chiumenti M. Smeared crack approach: back to the original track. Int J Numer Anal Methods Geomech 2006; 30:1173–1199.

[25] Feist C., Hofstetter G. An embedded strong discontinuity model for cracking of plain concrete. Comput Methods Appl Mech Engrg 2006; 195:7115–7138.

[26] Gasser T.C., Holzapfel G.A. 3D Crack propagation in unreinforced concrete. A two-step algorithm for tracking 3D crack paths. Comput Methods Appl Mech Engrg 2006; 195:5198–5219.

[27] Cervera M., Chiumenti M. Mesh objective tensile cracking via a local continuum damage model and a crack tracking technique. Comput Methods Appl Mech Engrg 2006; 196:304–320.

[28] Feist C., Hofstetter G. Mesh-insensitive strong discontinuity approach for fracture simulations of concrete. In: Proceedings of the 9th international conference on numerical methods in continuum mechanics, 2003.

[29] Jäger P., Steinmann P., Kuhl E. Modeling three-dimensional crack propagation - A comparison of crack path tracking strategies. Int J Numer Methods Engng 2008; 76:1328–1352.

[30] Clemente R. Análisis Estructural de Edificios Históricos mediante Modelos Localizados de Fisuración (in Spanish). Ph.D. Thesis. Technical University of Catalonia, 2007.

[31] Pela' L. Continuum Damage Model for Nonlinear Analysis of Masonry Structures. Ph.D. Thesis. Technical University of Catalonia, University of Ferrara, 2009.

[32] Lemaitre J., Chaboche J.L. Aspects phénoménologiques de la rupture par endommagement. J Méc Appl 1978; 2:317–365.

[33] Cervera M., Oliver J., Faria R.: Seismic evaluation of concrete dams via continuum damage models. Earthquake Eng Struct Dyn 1995; 24(9):1225–1245.

[34] Simó J.C., Ju J.W. Strain- and stress-based continuum damage models – I Formulation. Int J Solids Struct 1987; 23:821–840.

[35] Cervera M. Viscoelasticity and Rate-Dependent Continuum Damage Models. Monography Nº-79. CIMNE, Technical University of Catalonia, 2003.

[36] Bazant Z.P., Oh B.H. Crack band theory for fracture of concrete. Mater Struct 1983; 16:155–177.

[37] Oliver J. A consistent characteristic length for smeared cracking models. Int J Numer Methods Engng 1989; 28:461–474.

[38] Cervera M., Hinton E., Hassan O. Non linear analysis of reinforced concrete plate and shell structures using 20-noded isoparametric brick elements. Comput Struct 1987; 25(6):845-869.

[39] Cervera M., Agelet de Saracibar C., Chiumenti M. COMET: COupled MEchanical and Thermal analysis - Data Input Manual Version 5.0. Technical report IT-308. CIMNE, Technical University of Catalonia, 2002.

[40] GiD: the personal pre and post-processor. CIMNE, Technical University of Catalonia, 2002. Available from: http://gid.cimne.upc.es

[41] Rots J.G. Computational modelling of concrete fracture. Ph.D. Thesis. Delft University of Technology, 1988.

[42] Gálvez J.C., Elices M., Guinea G.V. and Planas J. Mixed mode fracture of concrete under proportional and nonproportional loading. Int J Fract 1998; 94:267-284.

[43] Gilbert M. RING masonry arch analysis software [last update: 29.04.05]. Available from: http://www.shef.ac.uk/ring

8. Figures Captions

Figure 1 Recent FEM approaches to crack modelling: a) X-FEM/E-FEM without regularization; b) regularized E-FEM [4]; c) regularized X-FEM [16].

Figure 2 SCA: a) classical [1] and b) embedded [18,19].

Figure 3 Location of cracks origin coordinates.

Figure 4 Exit point of element I (a); new potential element J and its entry point (b).

Figure 5 Crack "about-turn" in the proximity of the neutral axis, under bending conditions.

Figure 6 Maximum curvature criterion: a) tip element correction and b) neighbour elements chosen to compute V_c (with thickened sides).

Figure 7 Deformed mesh (x100) and tensile damage contour with a smeared damage model: mesh with average size $h_e = 5\,\text{mm}$ (a) and mesh with average size $h_e = 2.5\,\text{mm}$ (b).

Figure 8 Deformed mesh (x100) and tensile damage contour with the localized damage model: mesh with average size $h_e = 5\,\text{mm}$ (a) and mesh with average size $h_e = 2.5\,\text{mm}$ (b).

Figure 9 Load vs. displacement for holed strip with the localized damage model. Comparison among different mesh sizes.

Figure 10 Three point bending test setup [41].

Figure 11 a) Damage in the bending beam, b) detail of crack and c) deformed mesh (x35).

Figure 12 Load vs. displacement for bending beam. Comparison among different magnitudes of the analysis step.

Figure 13 Mixed-mode bending test setup [42].

Figure 14 Numerical deformed shapes (x100 and x300) at collapse and details of cracks: a) specimen 1 (three point test) and b) specimen 2 (four point test).

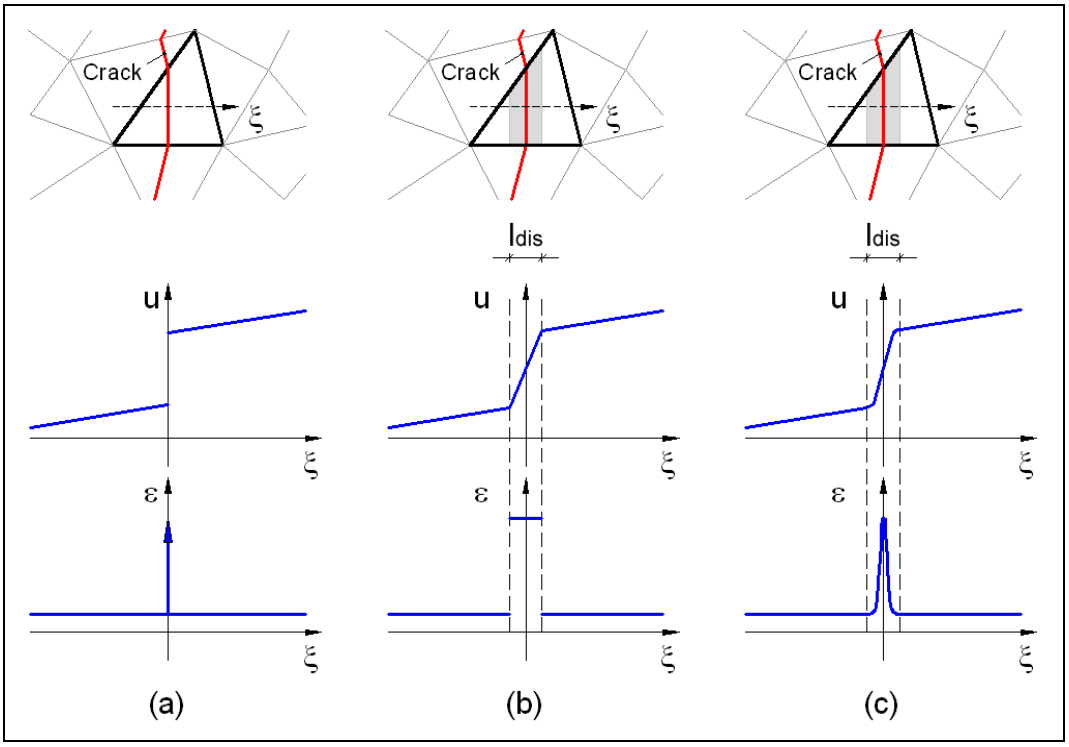

Figure 1 Recent FEM approaches to crack modelling: a) X-FEM/E-FEM without regularization; b) regularized E-FEM [4]; c) regularized X-FEM [16].

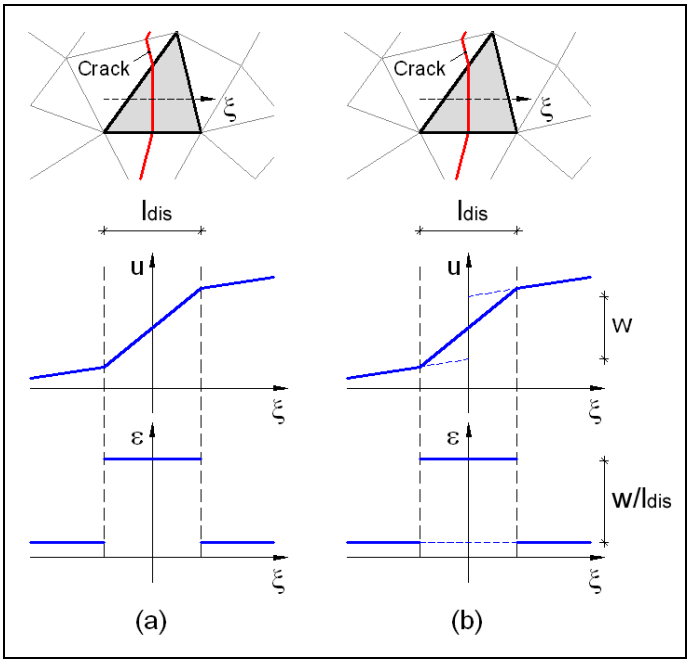

Figure 2 SCA: a) classical [1] and b) embedded [18,19].

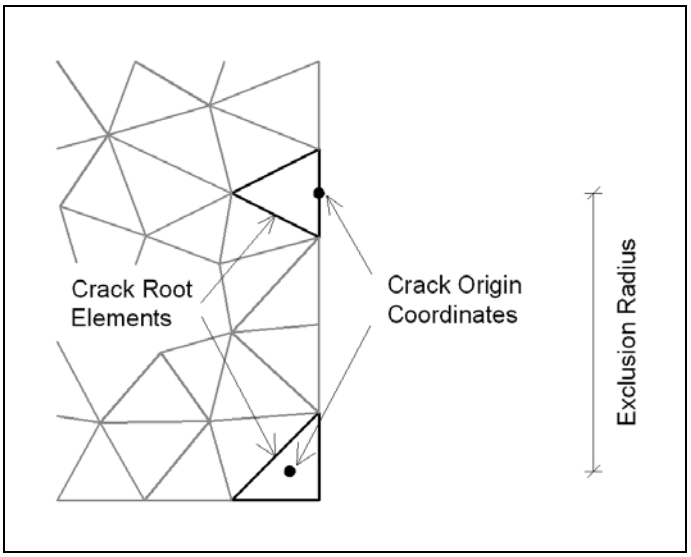

Figure 3 Location of cracks origin coordinates.

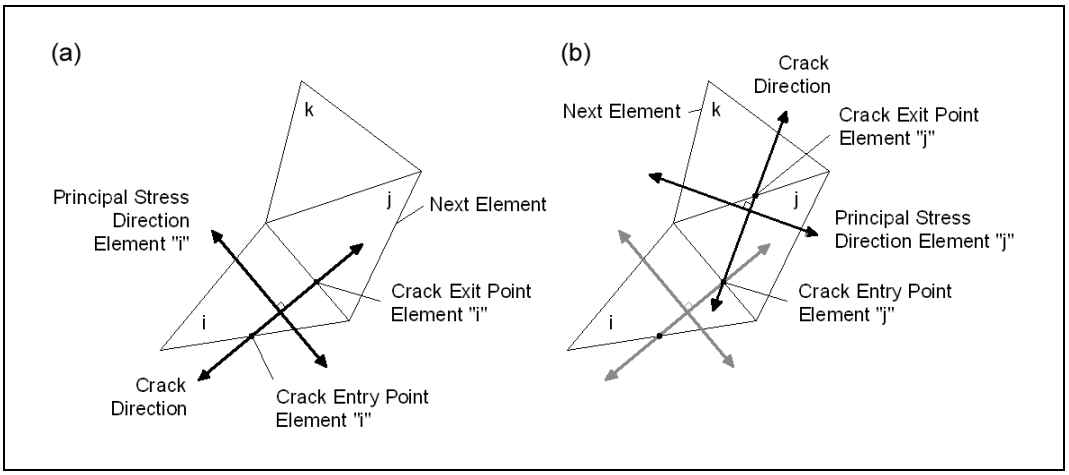

Figure 4 Exit point of element I (a); new potential element J and its entry point (b).

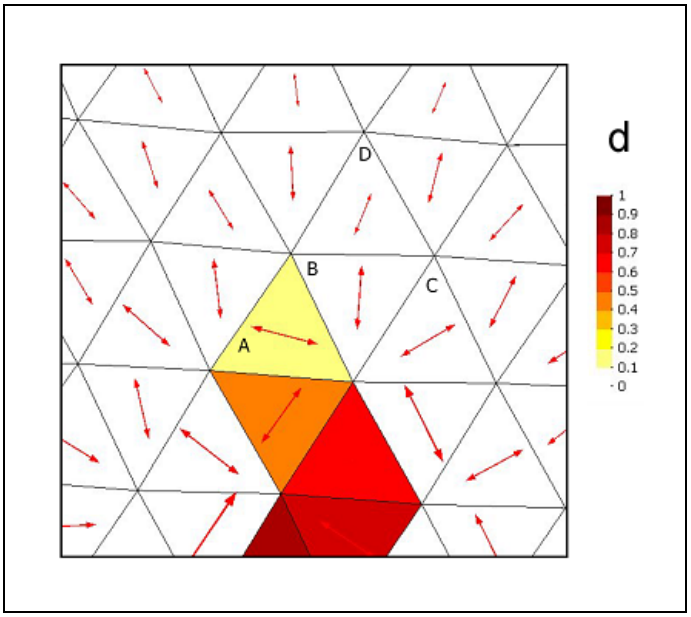

Figure 5 Crack "about-turn" in the proximity of the neutral axis, under bending conditions.

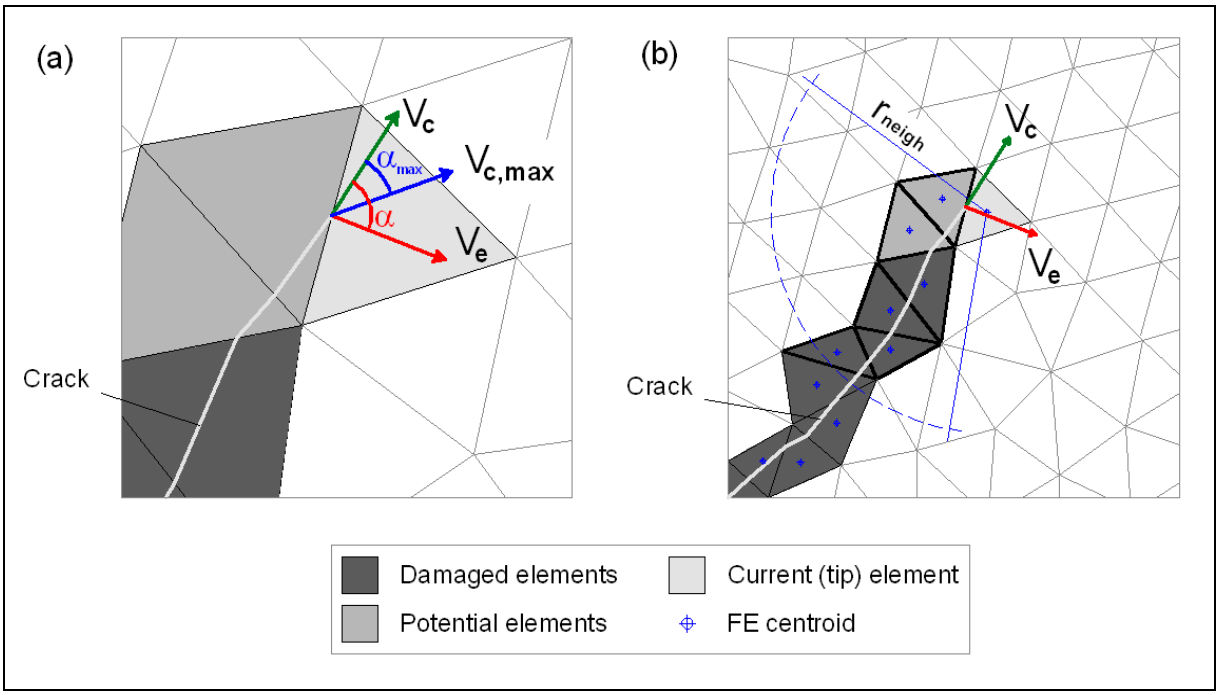

Figure 6 Maximum curvature criterion: a) tip element correction and b) neighbour elements chosen to compute V_c (with thickened sides).

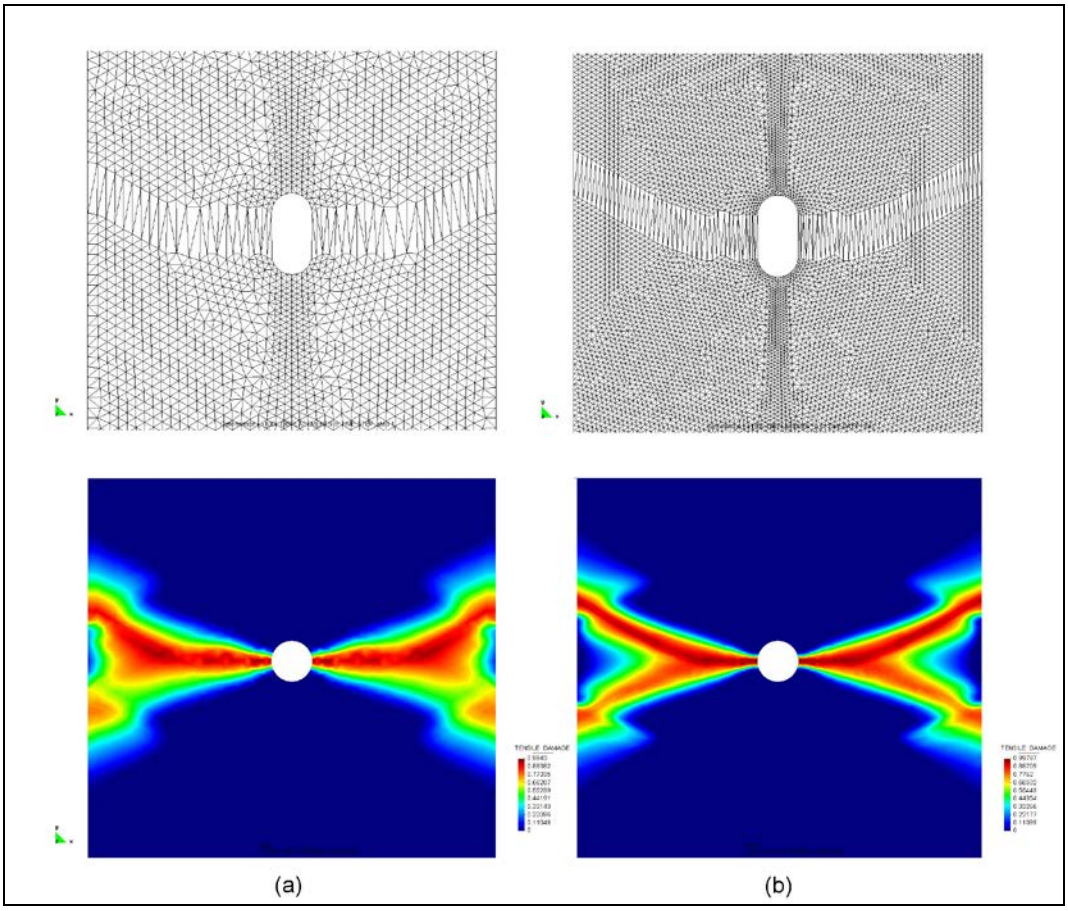

Figure 7 Deformed mesh (x100) and tensile damage contour with a smeared damage model: mesh with average size h_e = 5 mm (a) and mesh with average size h_e = 2.5 mm (b).

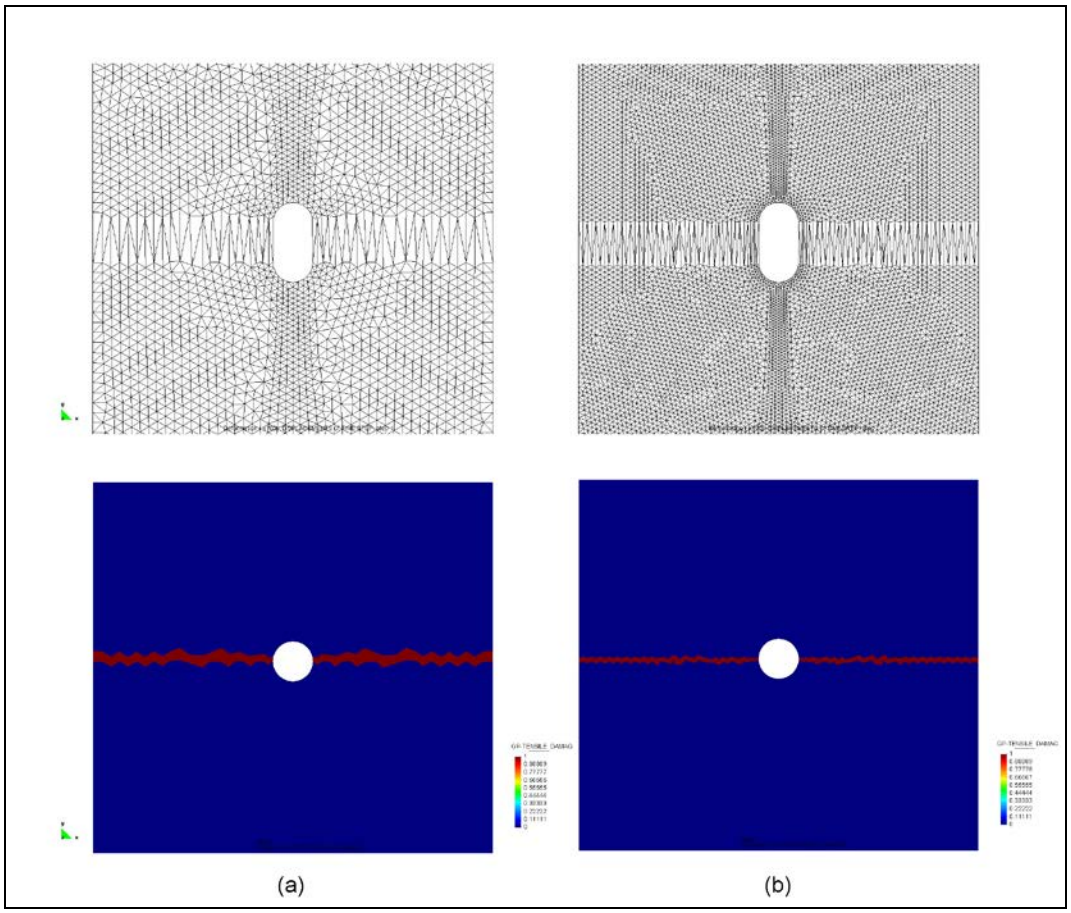

Figure 8 Deformed mesh (x100) and tensile damage contour with the localized damage model: mesh with average size h_e = 5 mm (a) and mesh with average size h_e = 2.5 mm (b).

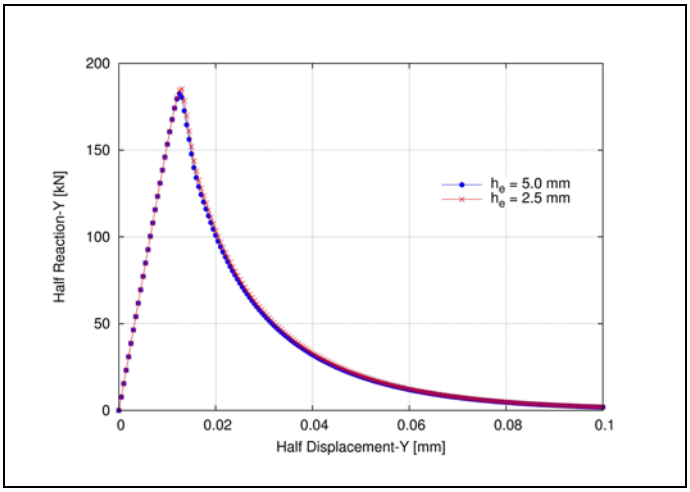

Figure 9 Load vs. displacement for holed strip with the localized damage model. Comparison among different mesh sizes.

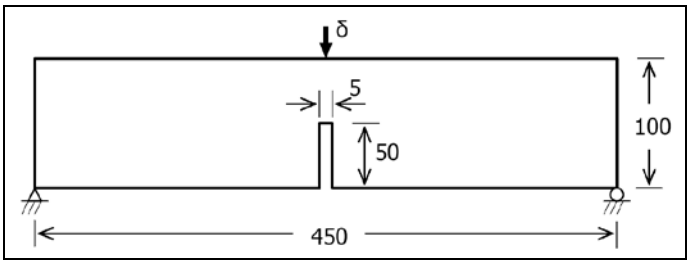

Figure 10 Three point bending test setup [41].

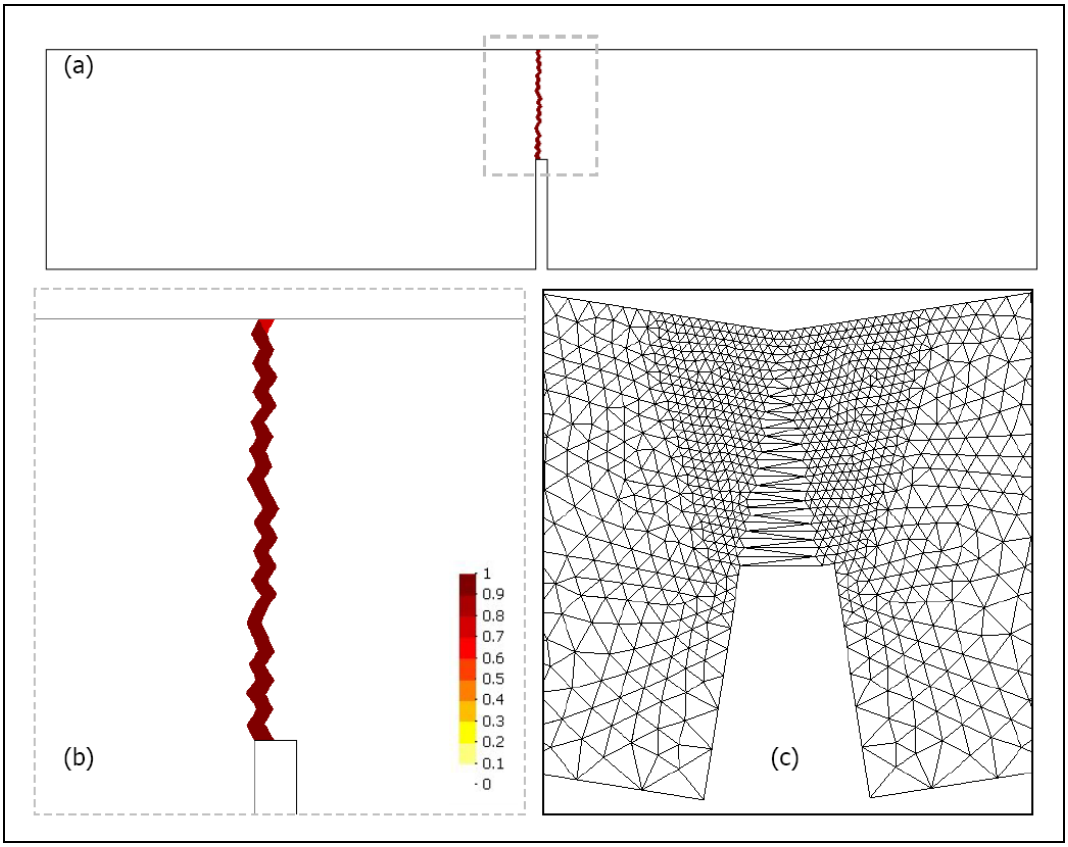

Figure 11 a) Damage in the bending beam, b) detail of crack and c) deformed mesh (x35).

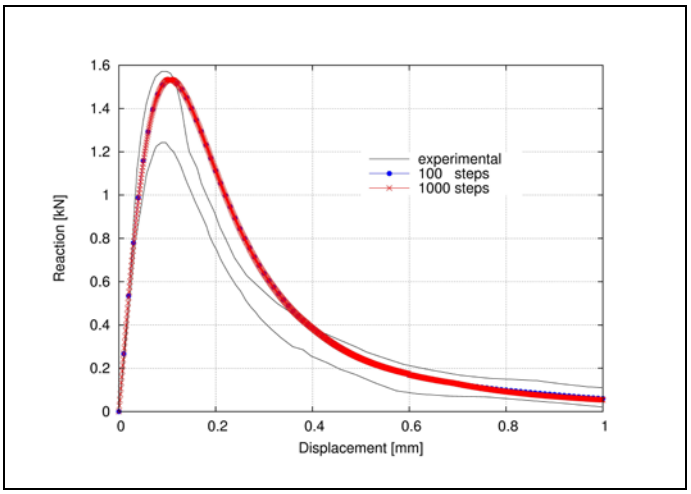

Figure 12 Load vs. displacement for bending beam. Comparison among different magnitudes of the analysis step.

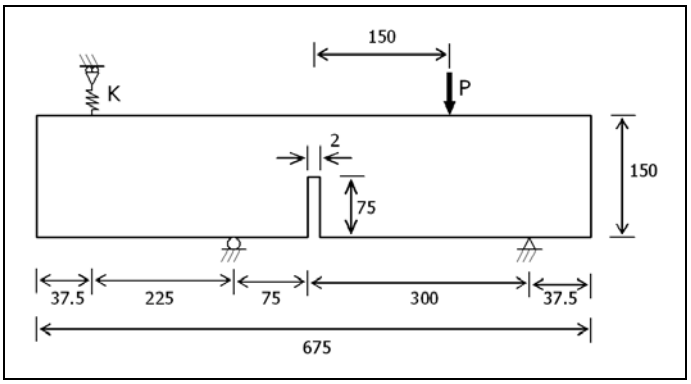

Figure 13 Mixed-mode bendig test setup [42].

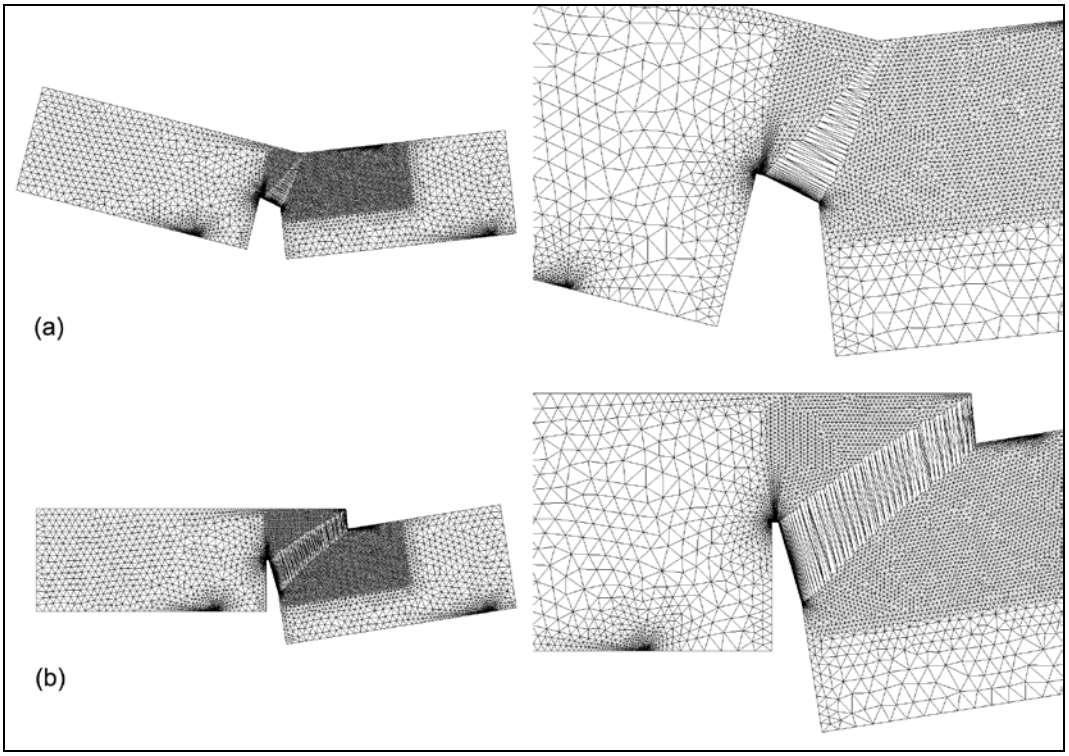

Figure 14 Numerical deformed shapes (x100 and x300) at collapse and details of cracks: a) specimen 1 (three points test) and b) specimen 2 (four points test).

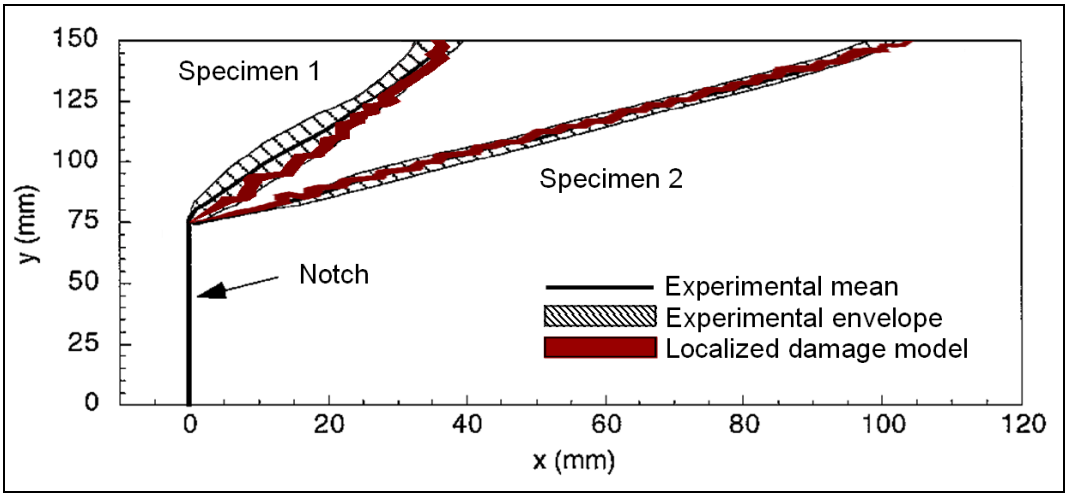

Figure 15 Comparison between the experimental and numerical crack tracks for the specimens 1 and 2.

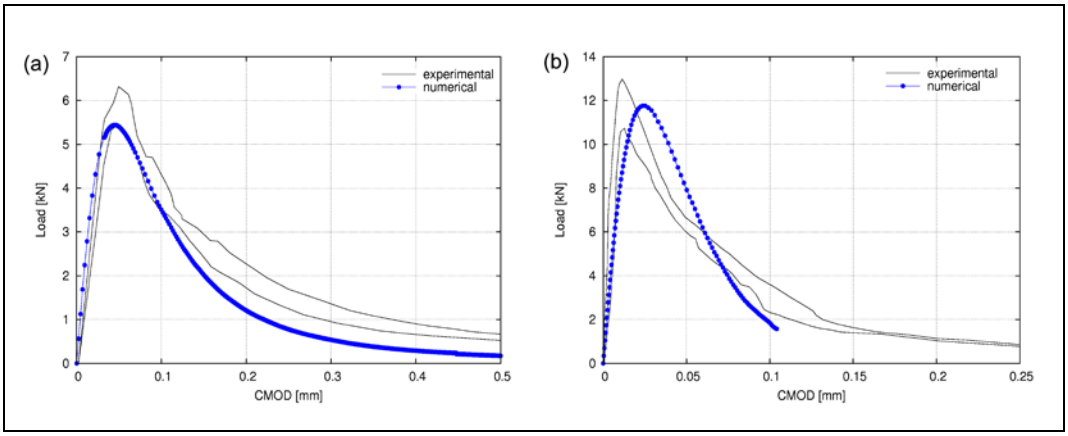

Figure 16 Load vs. CMOD for the specimen 1 (a) and the specimen 2 (b).

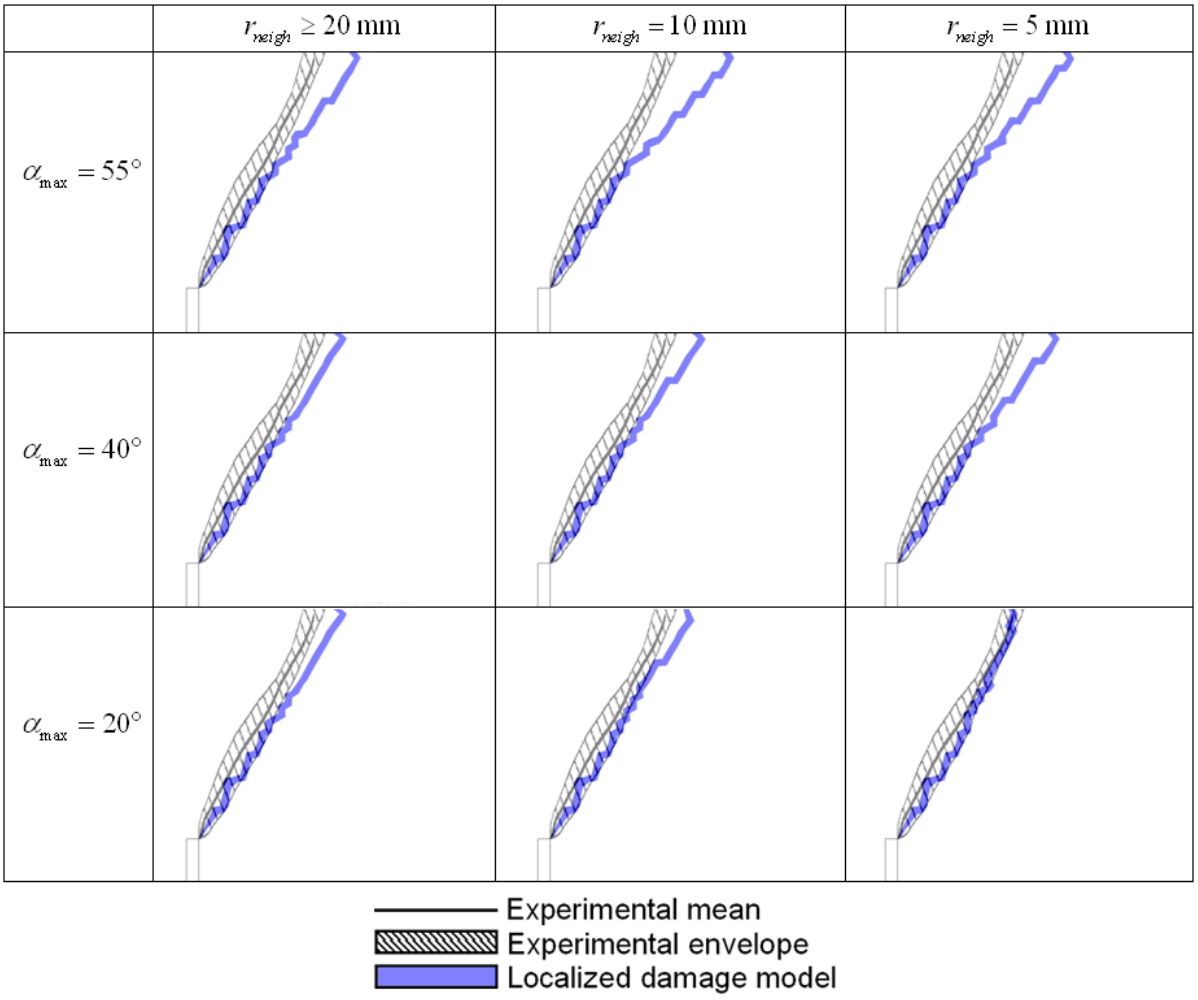

Figure 17 Specimen 1: numerical crack track sensitivity to r_{neigh} and α_{max}.

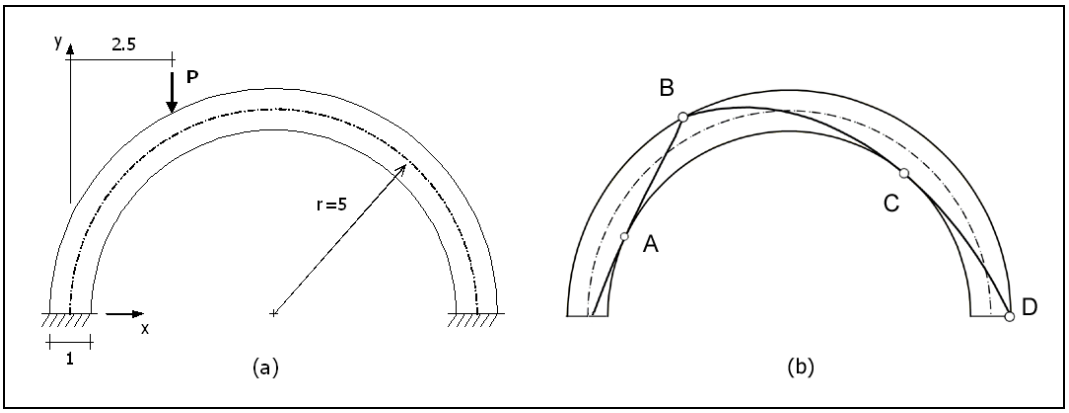

Figure 18 Semicircular masonry arch: a) geometry [m]; (b) thrust line and plastic hinges obtained via limit analysis [43].

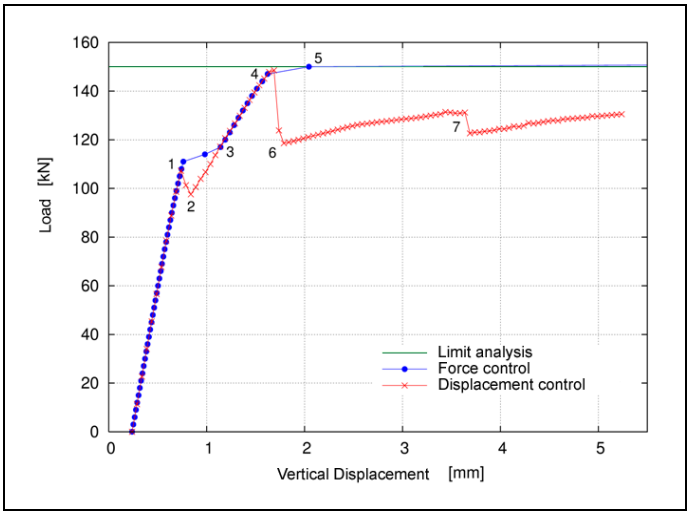

Figure 19 Comparison between Load vs. Vertical Displacement curves for limit analysis and smeared damage model under load or displacement control.

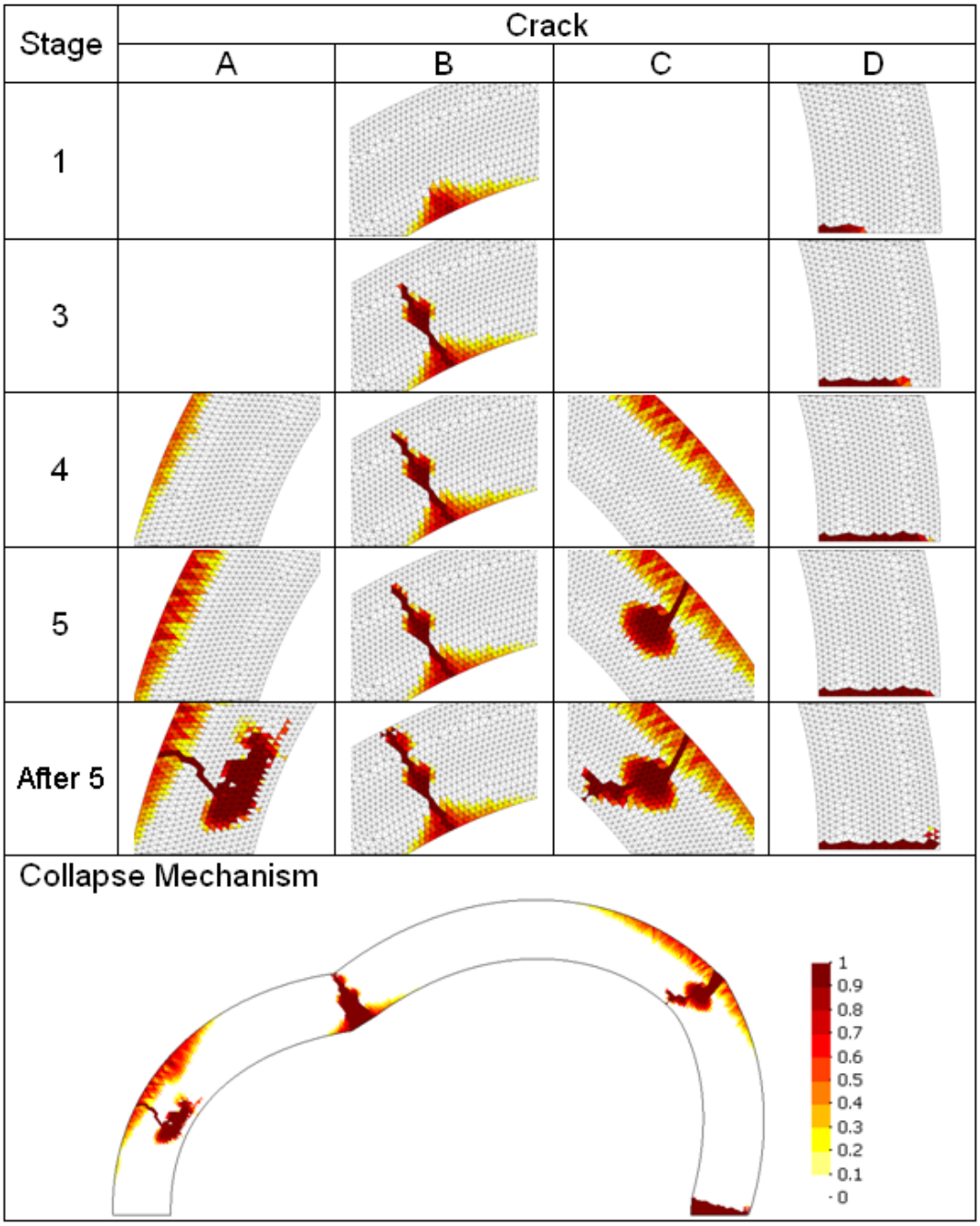

Figure 20 Smeared damage model (analysis under force control): cracks growth at different stages of the calculus and final collapse mechanism (amplification of mesh deformation: x100).

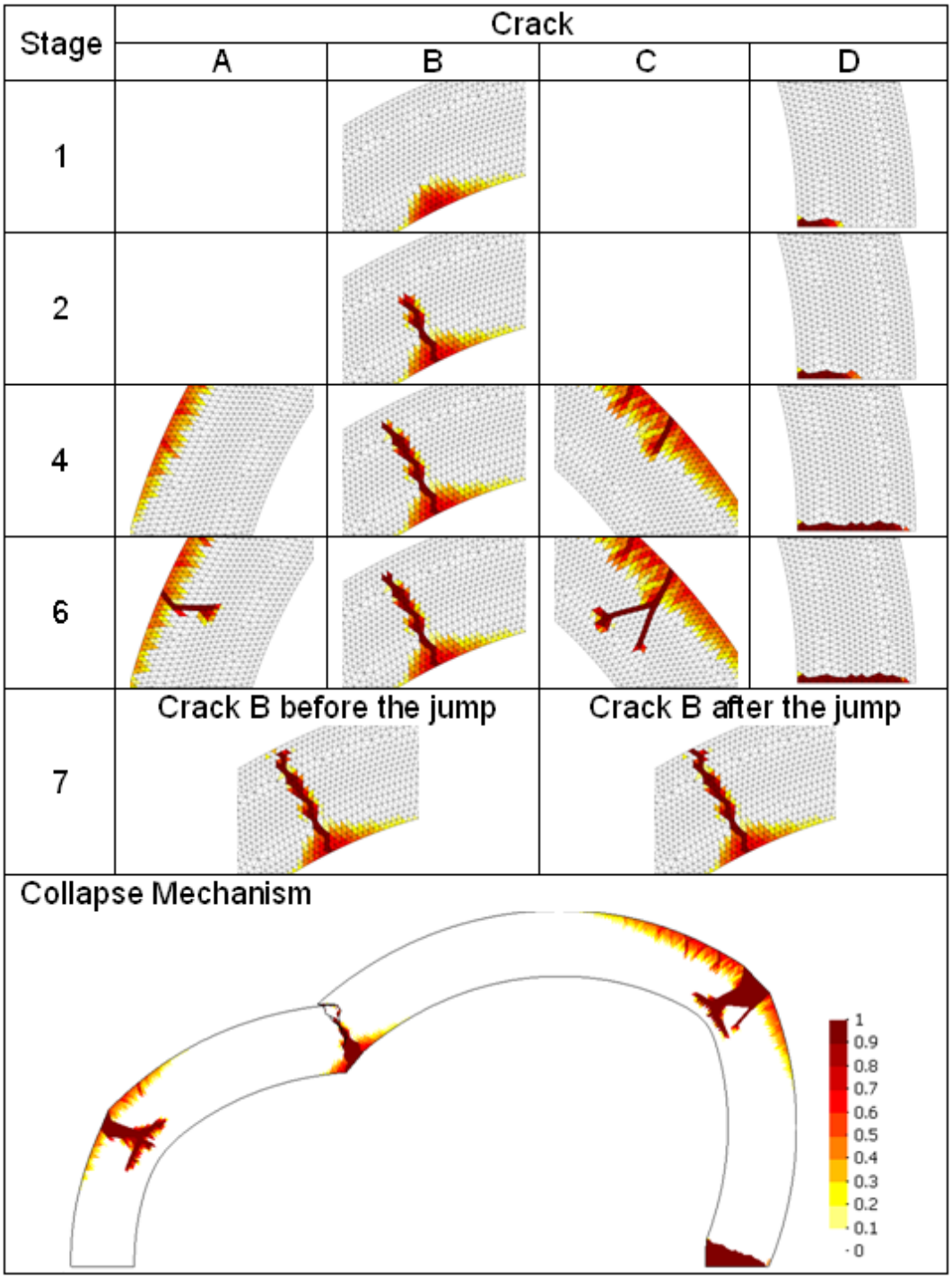

Figure 21 Smeared damage model (analysis under displacement control): cracks growth at different stages of the calculus and final collapse mechanism (amplification of mesh deformation: x100).

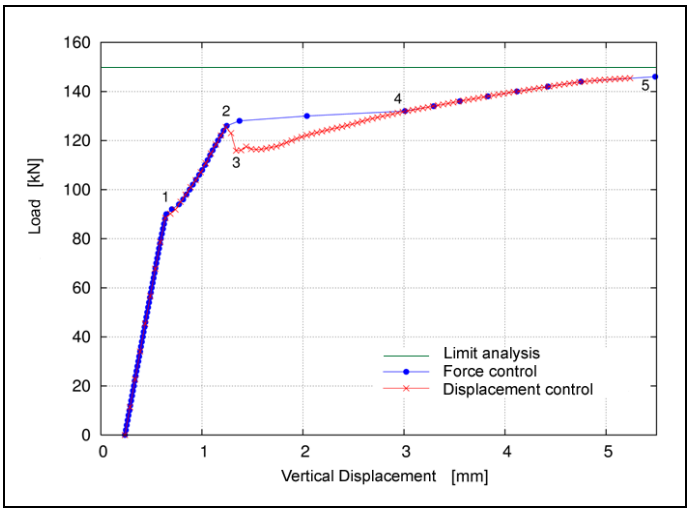

Figure 22 Comparison between Load vs. Vertical Displacement curves for limit analysis and localized damage model under load or displacement control.

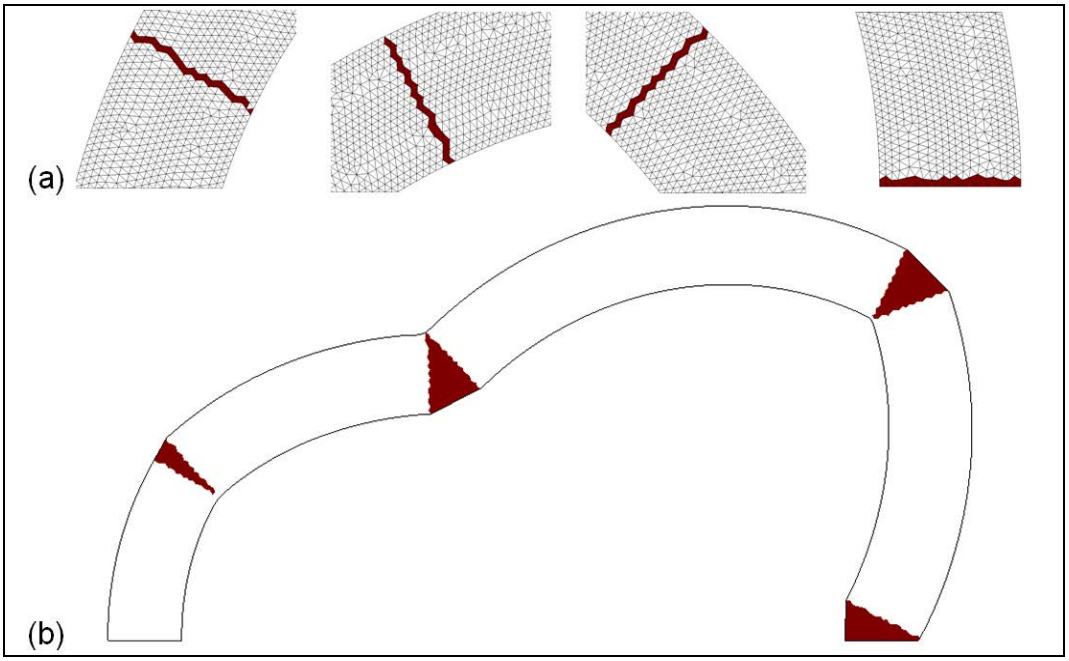

Figure 23 Localized damage model: a) detail of cracks at collapse and b) collapse mechanism (amplification of mesh deformation: x100).